Petrofabric Analysis of Potash Rocks, Esterhazy, Saskatchewan

A. R. Clark[1] and W. M. Schwerdtner[2]

ABSTRACT

Orientations were obtained, by means of a reflection goniometer for approximately 2000 grains of sylvite and halite in sylvinite specimens from the potash mines, Esterhazy, Saskatchewan. The orientation patterns for both halite and sylvite have orthorhombic symmetry, which corresponds with the symmetry of the gentle folds present in the study area.

A dynamic analysis of the fabric was made assuming that the evaporite beds behaved as rheids with a low creep strength. The observed state of preferred orientation is considered to be due to syntectonic crystallization, and Kamb's theory of preferred crystal growth under non-hydrostatic stress is applied.

The hypothetical fabric predicted by Kamb's theory agrees with the observed fabrics of halite and sylvite. Kamb's theory not only predicts the orientation patterns, but also predicts the equant grain shapes of both minerals and the larger grain size of sylvite.

INTRODUCTION

This paper presents results of fabric analyses of slightly deformed sylvinites from the Middle Devonian Prairie Evaporite Formation. One sample of a halite rock, from about 100 feet below the main potash seam, was also analyzed.

All samples were taken in the International Minerals and Chemical Corporation mine at Esterhazy, Saskatchewan. The main ore zone is about 3000 feet below ground level, and is about 12 feet thick. The samples from the ore bed consist of sylvite and halite, with variable amounts of clay and other insolubles.

Apparently, these rocks have not undergone any great tectonic deformation, and the observed fabrics are thought to have resulted from syntectonic crystallization. Kamb's (1959-1961) theory for crystal growth under non-hydrostatic stress can be applied and the validity of this approach can be assessed.

The writers gratefully acknowledge financial assistance from the National Research Council of Canada and the Saskatchewan Research Council. They would also like to record their thanks to the International Minerals and Chemical Corporation, Esterhazy, for granting them access to the mine for sampling. Thanks are also due to Dr. N. C. Wardlaw, University of Saskatchewan, for critically reading the manuscript, and the Saskatchewan Department of Mineral Resources, Records Branch, for making the drawings.

[1]California Standard Company, Calgary, Alberta.

[2]Department of Geological Sciences, University of Toronto. The work was carried out at the Department of Geological Sciences, University of Saskatchewan, Saskatoon, Saskatchewan.

PETROGRAPHY

The various sylvinite samples analyzed are from different stratigraphic levels within the main ore bed. Dolomite, illite, and chlorite (Wardlaw, personal communication, 1964) occur interstitially in variable amounts, with halite and sylvite.

Halite grains commonly occur in clusters, 3 to 5 inches across, but also occur as isolated grains which tend to be somewhat larger than those in the clusters. Grains are subhedral to euhedral, generally equant, and range from 0.1 to 2.0 inches in diameter with a 0.4 inch average. Halite occurs as both colorless and milky varieties. Many colorless grains contain milky patches, and microscopic examination indicates that the milky character is due to very small inclusions.

Sylvite grains, although approximately equidimensional, are generally very irregular in shape. The grains vary in size from 0.2 to 5.0 inches, with an average of about 0.75 inches. Grains vary from colorless, through orange, to dark red. Most grains are darker red towards their margins. Van der Plank (1962) observed that the red color is the result of fine iron oxide inclusions in the grains.

Irregular patches and veins of red-orange carnallite, up to two inches wide, are present in some of the specimens. It occurs in the interstices between the halite and sylvite grains, and commonly appears to corrode and penetrate them, suggesting replacement of halite and sylvite by carnallite. More conclusive evidence of replacement are thin veins of carnallite occurring preferentially along halite and sylvite cleavage planes.

The sample of rock salt collected below the main potash zone consists of massive halite, with irregular grey-green clay patches up to 5 inches across, present to about 10 per cent by volume. The halite grains are very irregular, though roughly equant, with serrated grain boundaries. The grains vary from 0.1 to 1.0 inches in diameter, with the larger grains occurring in the clay-rich portions. The grains are cream-colored in the clay-free rock, but more commonly are colorless where clay is present.

METHOD OF INVESTIGATION

Seven oriented samples of sylvinite were taken from faces recently cut by continuous mining machines. The orientation of cleavage faces, down to 0.1 inches diameter, was measured using a reflection goniometer (Fig. 1). Since both sylvite and halite are generally coarse-grained, large specimens are necessary to measure a statistical sample of grains, and at least 175 grains per sample were measured.

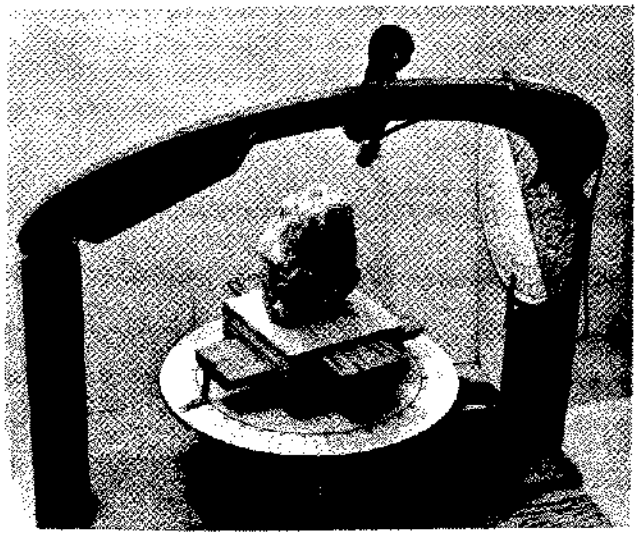

Figure 1. Reflection goniometer.

The goniometer is similar in design to one described by Clabaugh (1962). A small 5x telescope and light source are mounted at the centre of a 30-inch diameter wooden arc, which rotates about a horizontal axis (Fig. 1). The sample is mounted rigidly, with known orientation, in plaster of Paris, on a stage that rotates about a vertical axis. The stage can be moved both horizontally and vertically.

The cleavage face being measured must be located at the intersection of the telescope axis, horizontal axis, and vertical axis. This orientation is achieved by rotating the telescope to the horizontal position, then moving the specimen horizontally and vertically until the cleavage face is centred in the telescope.

The orientation of the pole to the cleavage face is found by rotating the specimen, and, at the same time, raising and lowering the telescope until a beam from the light source is reflected from the cleavage face back to the telescope. The inclination of the reflecting cleavage is recorded from the scale on the horizontal axis, as well as the azimuth of the cleavage face from the scale on the vertical axis.

A protractor reticle, mounted in the telescope, is used to measure the rake angle between the traces of the two cleavages on the (100) plane and the horizontal. The poles thus obtained represent the three crystallographic directions of the cubic crystals.

By chipping and gouging, imperfect cleavage faces can be greatly improved. By observing the manner in which a face breaks, reflecting surfaces which are not cubic-cleavage faces can be eliminated. Surfaces other than cubic planes generally have a poor quality of reflection.

Most specimens analyzed contained a set of vertical fractures parallel to the mine face from which they were taken. This fracturing is caused by the cutting action of the continuous mining machines. Special attention was paid to avoid measuring reflecting surfaces in crystals parallel to these fractures.

If two reflecting surfaces of a grain, each containing two visible sets of cleavage traces, are measured, it is possible, by use of a Wulff net, to check that these are (100) planes. If the first reflecting surface (S_1) is a cubic cleavage plane, but the other one is a non-cubic surface, then the poles of the cleavage traces on S_2 will include, in most cases, angles of more than 90 degrees. Thus, a rigorous distinction between cubic and non-cubic surfaces is possible if we draw two great circles, each connecting one cleavage trace on S_1 with one trace on S_2. These circles will represent cubic planes, and the two cleavage traces on S_1 will be the normals to the cubic planes.

The samples were broken along subhorizontal surfaces at least two inches apart to avoid measuring the same grain twice. Grains larger than two inches were given special attention to exclude repeating measurements. The specimens broke along highly irregular surfaces and every grain possible, on each surface so exposed, was measured in order to establish a uniform practice.

All three crystallographic axes, of all grains measured, were plotted. The petrofabric diagrams were constructed on a Schmidt equal area net, and the contouring was done according to the method described by Haff (1938). The peripheries of the diagrams parallel the bedding of the strata in all cases.

Diagrams containing only poles of the large grains were constructed for some samples as well as the conventional nonselective diagrams. Some selective diagrams containing poles of large grains only were contoured using the Mellis method (Mellis, 1942; Flinn, 1958).

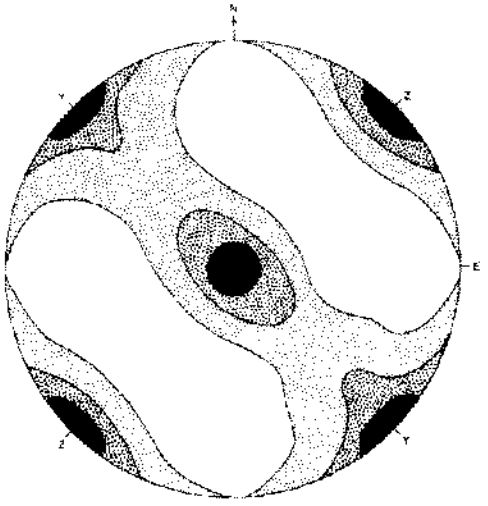

Figure 2. Schematic distribution of the crystallographic axes predicted by Kamb's theory for $(p_y - p_x) < (p_z - p_y)$.

Diagrams for each sample were drawn with [[100]] poles weighted with respect to the volume of the grains. Since the halite and sylvite grains are approximately equant, an estimate of their volumes can be made from the cubes of their linear dimensions. Grains smaller than 0.03 cubic inches are not very common and this volume was chosen as a unit volume. The number of unit volumes in each grain was recorded as a figure on the equal area net in the positions of the [[100]] poles of the measured grains. Grains smaller than 0.03 cubic inches were neglected as they had practically no bearing on the contours in the weighted diagrams. Each of these contours represents a percentage of the total number of unit volumes plotted on any diagram.

The weighted diagrams for all of the sylvinite samples were combined in a composite diagram [Fig. 3). Separate composite-weighted diagrams were also constructed (Figs. 4, 5).

RESULTS

Irregular, elongate minima, trending approximately NW-SE, are developed in each diagram. In most diagrams there is also a tendency for elongate minima trending NE-SW. Both systems tend to interfinger. The outline of the minima clearly indicates the anisotropic nature of the fabrics, although they do not describe the "preferredness" of the orientation (Chayes, 1949).

Most diagrams contain more than one maximum. While the point density in the maxima of the conventional diagrams hardly exceeds 5 per cent the maxima of the weighted diagrams have densities of 10 per cent or more. It should be noted, also, that the maxima are usually larger in the weighted diagrams.

Flinn (1958) showed that a preferred orientation on a petrofabric diagram can be established by showing that the orientation patterns obtained have a significant deviation from the pattern containing points of random orientation. He discusses several statistical tests of significance. These tests are designed for diagrams on which each grain is represented by a single pole and cannot be applied readily to the diagrams for halite or sylvite (three a-crystallographic axes per grain).

In statistically homogeneous fabrics, a number of partial diagrams prepared from the same specimen are compared with each other and similarities are accepted as due to preferred orientation in the specimen (Ingerson, 1940). In order to make such comparisons, the statistic homogeneity of a fabric has to be established.

Two partial diagrams, for the large grains in the upper and lower half of sample A, were prepared. The larger grains were about 10 per cent more abundant in the lower part of the sample. The patterns of the two partial diagrams (Figs. 6c, 6d) are very similar, and the fabric of the large grains is considered as statistically homogeneous.

The poles of all large grains measured in the total specimen are represented in Fig. 6e, which again shows a pattern similar to those of the two partial diagrams (Figs. 6c, 6d). The close similarity of the fabric patterns in the diagrams for the large grains, compared with the nonselective diagram of sample A (containing all grains measured), suggests a preferred orientation in sample A.

For the halite rock of sample H two partial nonselective diagrams were constructed for the upper and lower half of the sample. The close similarity of both partial diagrams shows that the fabric of sample H is statistically homogeneous. Again the conventional diagram (Fig. 13e) containing all the large grains of the total sample is very similar to each of the two partial diagrams, which indicates a preferred orientation of halite in the halite rock.

DISCUSSION OF THE PETROFABRIC DIAGRAMS

The interpretation of petrofabric diagrams is usually somewhat subjective, since there are numerous small inhomogeneities in any statistically homogeneous fabric, which tend to blur the patterns of preferred orientation. The influence of local inhomogeneities decreases as the sample size is increased and larger numbers of grains are measured.

Assuming statistic homogeneity for the rocks in the total mine are studied, the pattern of preferred orientation should be best defined in the composite diagrams (Figs. 3, 4, 5).

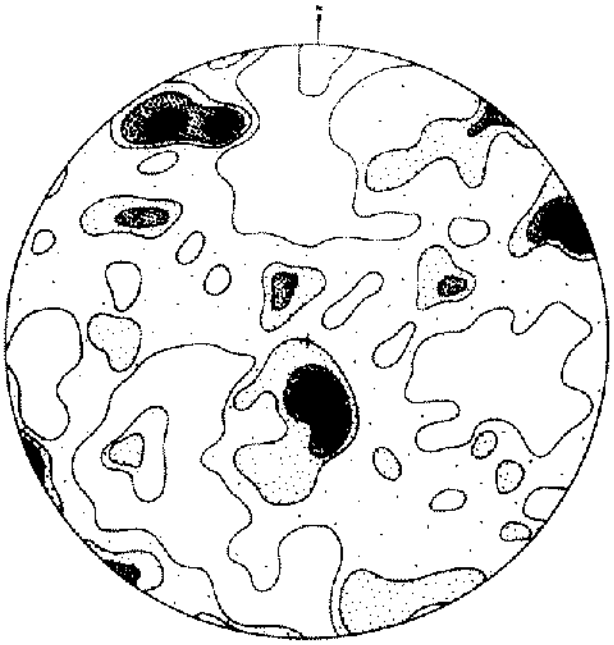

Figure 3. Composite diagram (size-weighted). 4680 Poles of ((100)) of halite and sylvite, > 10 - 6 - 4 - 2 - 0.

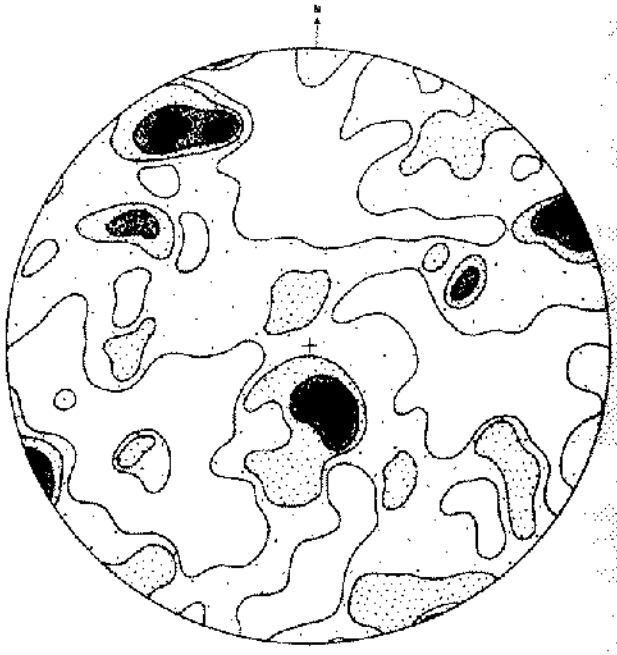

Figure 4. Composite diagram (size-weighted) for sylvite. 2091 Poles of ((100)), > 10 - 6 - 4 - 2 - 0.

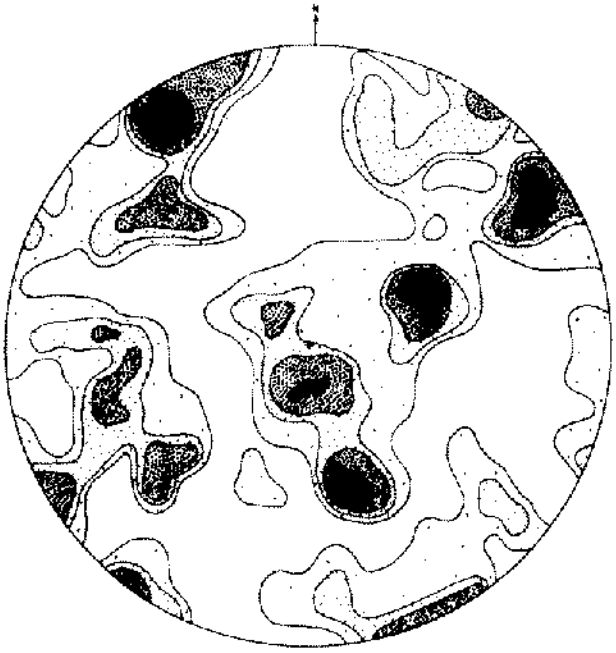

Figure 5. Composite diagram (size-weighted) for halite. 2589 Poles of ((100)), > 10 - 6 - 4 - 2 - 0.

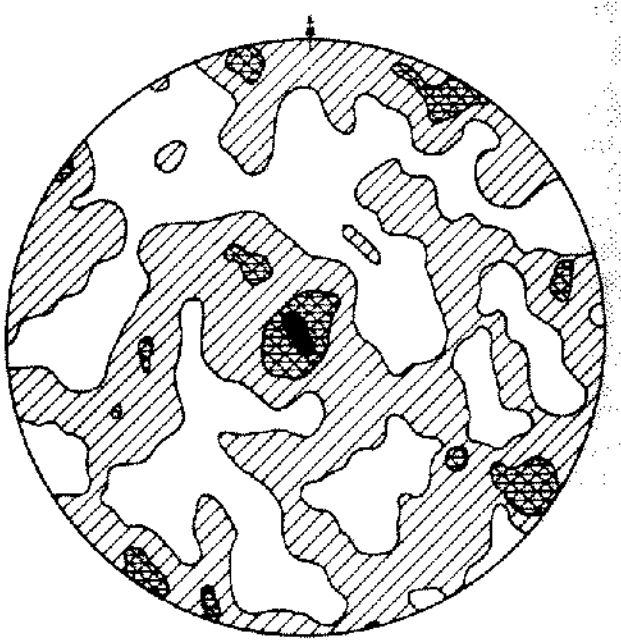

Figure 6a. Conventional diagram for 110 sylvite and 112 halite grains of sample A, > 3 - 2 - 1 - 0.

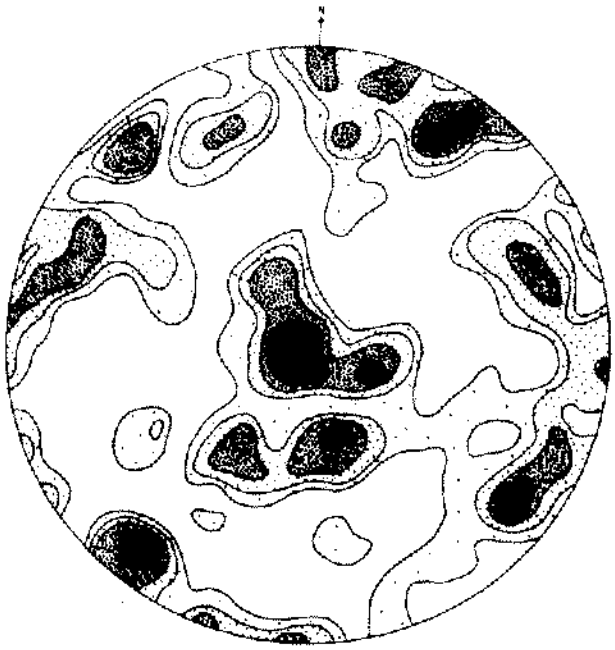

Figure 6b. Size-weighted diagram for all grains of sample A. > 10 - 6 - 4 - 2 - 0.

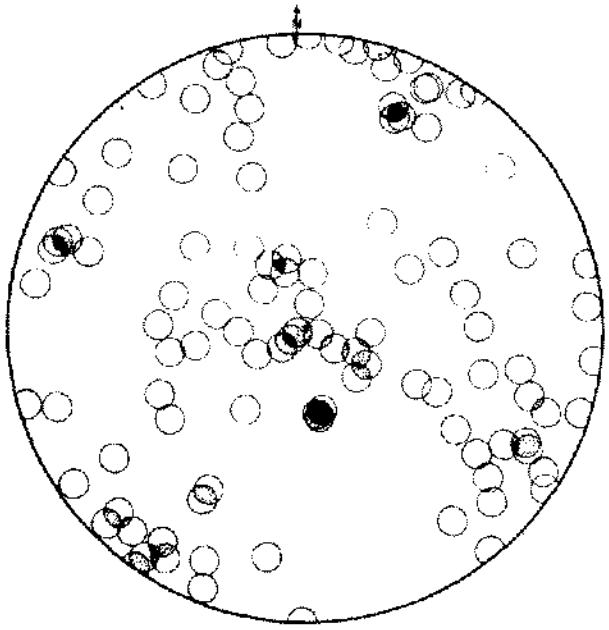

Figure 6c. 105 Cleavage poles of 35 large grains (> 0.75 inches across) in the upper half of sample A. > 5 - 4 - 2 - 0.

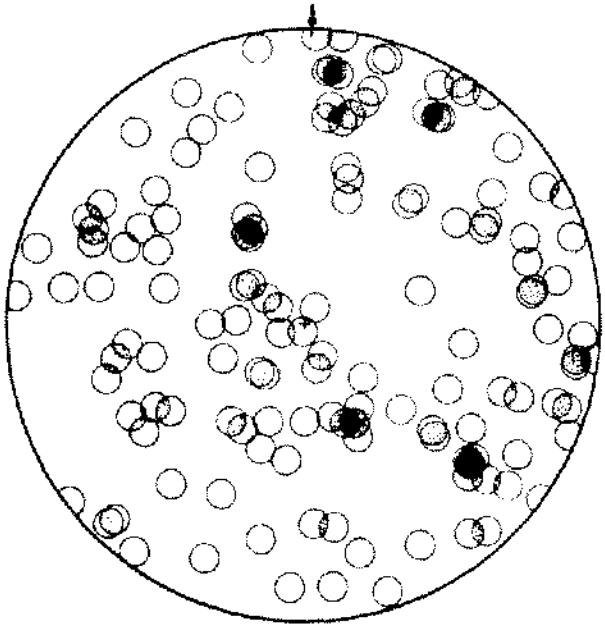

Figure 6d. 138 Cleavage poles of 46 large grains (> 0.75 inches across) in the lower half of sample A. > 10 - 8 - 5 - 2 - 0.

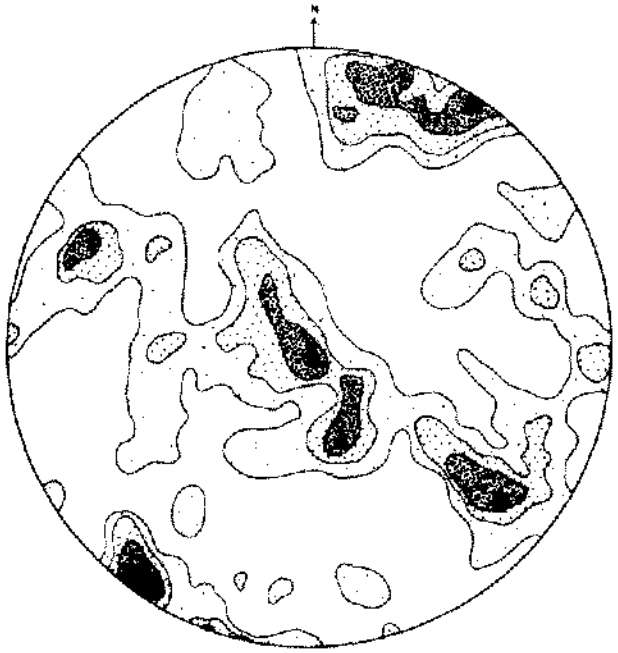

Figure 6e. Diagrams 6c and 6d combined (243 poles). > 4 - 3 - 2 - 1 - 0.

The weighted composite diagram, for all the sylvite and halite grains measured, has three maxima and a distinct girdle trending NW-SE (Fig. 3). There is also a tendency for the NE-SW girdle and a horizontal girdle (along the periphery of the diagram). Both the composite diagram for all sylvite grains (Fig. 4) and the composite diagram for all halite grains are similar to Fig. 3.

The fabric patterns of most weighted diagrams for the individual samples tend to be similar to those of the composite diagrams, thus indicating statistical homogeneity of the fabric over the total range of the sampling. The weighted diagram for sample D shows little similarity with Fig. 3, and the irregularity might reflect a local inhomogeneity of the fabric-creating factors.

Many of the conventional diagrams resemble the composite diagrams, although some lack a pronounced maximum. A tendency for the NW-girdle is always recognizable.

All diagrams exhibit pseudo-orthorhombic symmetry with three planes of symmetry: the horizontal plane, and two vertical planes tending NW-SE and NE-SW.

Although the potash beds lie almost horizontally there are some gentle folds west of the mine shaft (maximum dip of the beds is 6 degrees). All specimens analyzed were taken from quasi-horizontal beds in this general area.

The fold axes tend NW-SE and thus correspond with the major girdle in the petrofabric diagrams. The gentle macroscopic folds (Turner and Weiss, 1963, p. 154) have pseudo-orthorhombic symmetry (Sander, 1948; Engels, 1959, pp. 43-45) with their a-axes vertical and their b- and c-axes horizontal, trending NW-SE and NE-SW. Thus, there is complete correspondence between the symmetry of folds and that of the fabrics. The coincidence of crystallographic axes with the fold axes suggests that there is a true preferred orientation of halite and sylvite.

MECHANICS OF PREFERRED ORIENTATION OF SYLVITE AND HALITE

A preferred orientation of grains in a polycrystalline solid can arise during mechanical deformation, or as a result of annealing crystallization. Preferred orientations arising during mechanical deformation are due to either intracrystalline gliding combined with rotation of individual grains, or to syntectonic crystallization (Turner and Weiss, 1963, pp. 325, 353).

It is known from experiments that a preferred orientation due to intracrystalline gliding and grain rotation can only be detected after large distortion of the initial body (Barrett, 1952, pp. 442-484; Turner and Weiss, 1963, pp. 322-363). Subsequent annealing crystallization tends to change the pattern of preferred orientation. Experimental evidence suggests that only those polycrystalline aggregates which underwent a large distortion may develop a regular pattern of preferred orientation due to annealing (Turner and Weiss, 1963, p. 333).

It is clear that the potash rocks of Esterhazy have undergone very little distortion, since the bedding is essentially horizontal and there are locally numerous quasi-vertical veins of carnallite (Schwerdtner, 1964, Fig. 2). Unfortunately, little is known about the relative age of the carnallite veins, which might have been formed during, or after, a lateral distortion of the potash beds.[3]

Let us assume that the total distortion of the potash beds is indicated by the gentle folds described above. Such a slight deformation, which is not even apparent in the quasi-horizontal beds, could hardly create a preferred orientation due to intracrystalline gliding and grain rotation. It appears that the observed fabric could only result from syntectonic crystal growth in preferred directions.

Kamb (1959) has developed a thermodynamic theory for such competitive crystal growth under non-hydrostatic stress. In order to apply his theory, the directions of maximum, intermediate and least principal stress, in the rock, must be known together with the moduli of compliance for a given mineral.

[3] There is evidence for NW/SE-trending transcurrent faults in southeastern Saskatchewan (Hajtes, T. B., 1960, Alberta Soc. Petroleum Geologists Jour., vol. 8, pp. 33-73).

Carey (1953, pp. 91-92; 1962, p. 98) has discussed the dynamics of rheid folding in isotropic materials. He pointed out that deeply buried salt rocks behave as pseudo-viscous media, in tectonic processes involving low-strain rates (Carey, 1953, p. 69). It can be assumed that the stress field during the formation of the gentle folds was not controlled by the bedding, because the boundaries between rock salt and sylvinite are gradational and the clay material present in some units of the main potash zone is well disseminated.

The stress environment of the gentle folds[4] (Carey, 1953, p. 91) can be described by a triaxial ellipsoid whose shortest axis x is vertical (easiest relief) and whose intermediate axis y coincides with the slightly arcuate fold axis (intermediate relief). Following the convention in thermodynamics, tensile stresses are designated as positive and compressive stresses as negative.

Rheids at rest cannot support any shearing stress for durations above their rheidity (Carey, 1953). This may lead to the belief that the state of stress in the quasi-horizontal sylvinites was always hydrostatic, except for periods shorter than the rheidity. However, if the sylvinites were stressed below their creep strength (Turner and Weiss, 1963, p. 309) they were able to support a shearing stress indefinitely without any appreciable amount of permanent deformation.

Little information on the creep strength of salt and potash rocks has been published. Serata and Gloyna (1960, p. 2981) stated that the creep strength of rock salt decreases with an increase of the observation period, and that this creep strength is a logarithmic function of time. Similarly, the rate of creep decreases greatly with decreasing differential stress and increasing confining pressure (Ode, 1962). It thus appears irrelevant whether there is a fundamental strength of sylvinite, or whether the equivalent viscosity at very low creep rates and considerable confining pressure becomes extremely high. The total amount of permanent deformation will be small and hence the deformation is essentially elastic.

The directional agreement of fold axes and axial planes with the grain fabric in the quasi-horizontal sylvinites supports the assumption that the same stress environment gave rise to the gentle folds and the grain fabric in the quasi-horizontal beds. It further appears that the horizontal sylvinites transmitted a shearing stress when essentially elastically stressed, whereas the folded beds started to flow when stressed sufficiently above their creep strength. The non-hydrostatic state of stress, in the quasi-horizontal potash rocks, should then be reflected in the grain fabric.

The statistic homogeneity of the grain fabric throughout the total area studied suggests that the stress distribution in the sylvinites, which gave rise to the preferred grain orientation, was statistically homogeneous.

Kamb (1959) has applied his theory to the case of crystal growth in uniaxial stress fields. In general, the most stable orientation of a crystal is that for which the chemical potential across the interface normal to the greatest principal pressure is a minimum. This position can be determined by subtracting the chemical potential μ^u (crystallographic axes parallel to principal pressures) from μ^* (crystallographic axes inclined to principal pressures) and subsequently minimizing the equation so obtained (Kamb, 1959, p. 162).

There are two independent variables in Kamb's equations, the principal pressures (negatives of the principal stresses) and the direction cosines which define a given position of a crystal with respect to the principal axes. Kamb succeeded in normalizing his equations with respect to the principal pressures ($P_x = P_y$; P_z) which appear as Δ_p^2 in his equations. Kamb's absolute potential differences are thus independent of the sign of Δ_p.

Only the relative potential differences are needed to determine the direction of preferred crystal growth. For a given mineral at a given temperature, in a uniaxial stress field, these differences in Kamb's equations depend solely on the direction cosines.

In a triaxial stress field it is convenient to compare chemical potentials across crystal faces while all three crystallographic axes lie within the principal planes of stress. Three cases will

[4] These folds have recently been identified as "salt horses" (see K. O. Linn, this symposium), where concentrated brines infiltrated the ore zone from below. This resulted in a lowering of the creep strength.

be considered: the a_1-crystallographic axis coinciding with x (equations 1, 4), a_1 coinciding with y (2, 5), and a_1 coinciding with z (3, 6). While a_1 remains fixed, a_2 and a_3 rotate within the principal planes. Equations (1 - 6) were derived from Kamb (1959, equations 1, 9, 10, 11, 35) and Nye (1960, p. 160, table 9).

Equations (1 - 3) are valid for rocks which are composed of more than one mineral, whereas (4, 5, 6) describe the preferred orientation of a_2 and a_3 within the (yz), (xz), and (xy) planes for monomineralic fabrics containing small amounts of "impurities." Crystal growth proceeded without intergranular fluids (Kamb, 1959, section VI).

$$\mu_z^{\alpha} - \mu_z^{\alpha} = V_o \left(-S_{11} + S_{12} + \frac{S_{44}}{2}\right) \sin^2 \alpha \cos^2 \alpha \left(P_y - P_z\right)^2 \quad (1)$$

$$\mu_z^{\alpha} - \mu_z^{\alpha} = V_o \left(-S_{11} + S_{12} + \frac{S_{44}}{2}\right) \sin^2 \alpha \cos^2 \alpha \left(P_x - P_z\right)^2 \quad (2)$$

$$\mu_z^{\alpha} - \mu_z^{\alpha} = V_o \left(-S_{11} + S_{12} + \frac{S_{44}}{2}\right) \sin^2 \alpha \cos^2 \alpha \left(P_x - P_y\right)^2 \quad (3)$$

$$\bar{\mu}_z^{\alpha} - \bar{\mu}_z^{\alpha} = V_o \left(-S_{11} + S_{12} + \frac{S_{44}}{2}\right) \sin^2 \alpha \cos^2 \alpha \left(P_y - P_z\right)^2 \quad (4)$$

$$\bar{\mu}_z^{\alpha} - \bar{\mu}_z^{\alpha} = V_o \left(-S_{11} + S_{12} + \frac{S_{44}}{2}\right) \sin^2 \alpha \cos^2 \alpha \left(P_x - P_z\right)^2 \quad (5)$$

$$\bar{\mu}_z^{\alpha} - \bar{\mu}_z^{\alpha} = V_o \left(-S_{11} + S_{12} + \frac{S_{44}}{2}\right) \sin^2 \alpha \cos^2 \alpha \left(P_x - P_y\right)^2 \quad (6)$$

S_{ij} = moduli of compliance.

V = specific volume (per mole) of a crystal in a reference state.

μ_z^{α} = chemical potential across face normal to p_z, crystallographic axes parallel to principal pressures ($p_x < p_y < p_z$).

μ_z^{α} = chemical potential across face normal to p_z, [100] inclined to p_z.

$\bar{\mu}$ = mean chemical potentials across the three interfaces normal to principal axes.

α = angle between crystallographic axes and principal axes.

Note that the right sides of (1) and (4), (2) and (5), (3) and (6) are identical, which indicates identical preferred orientation for a given mineral in monomineralic and polymineralic fabrics. Let α vary to minimize equations (1-6). $(-s_{11} + s_{12} + \frac{s_{44}}{2})$ for halite is 11×10^{-13} cm^2/dyne, for sylvite 29×10^{-13} cm^2/dyne (Kamb, 1959, table 2). Equations (1-6) have their maximum values for $\alpha = \frac{\pi}{4}$, and their minimum values for α equal to zero or $\frac{\pi}{2}$. The most stable position for halite and sylvite is that with their crystallographic axes parallel to the principal axes of stress.

It is clear that the maximum differences in chemical potential will determine the degree of preferred orientation for halite and sylvite. In the sylvinite samples, both minerals grew under the same stress conditions and the maximum potential difference depends only on the values for $(-s_{11} + s_{12} + \frac{s_{44}}{2})$ and V_o. It is known that the maximum potential difference for sylvite is more than three times as great as that for halite. It follows that sylvite has a greater tendency than halite to develop the theoretical pattern predicted by Kamb's theory.

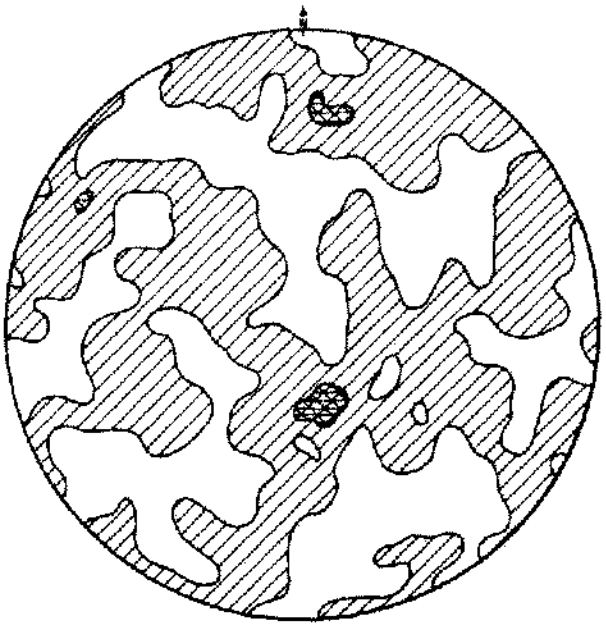

Figure 7a. Conventional diagram for 196 sylvite and 131 halite grains of sample B, > 2 - 1 - 0.

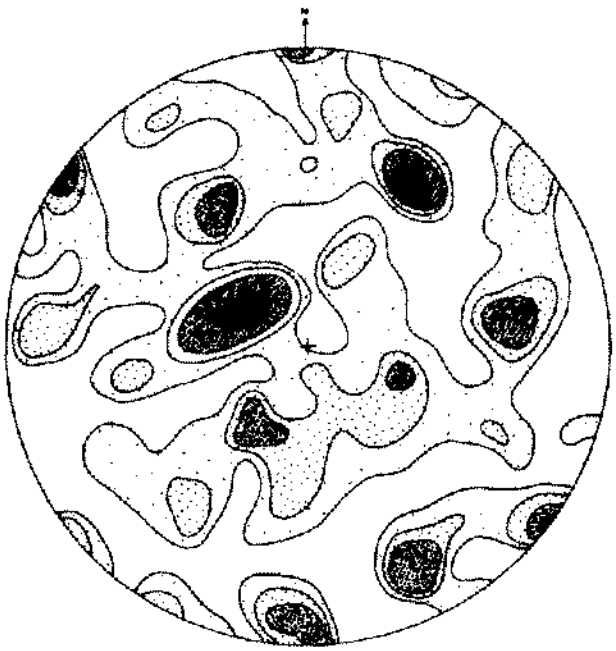

Figure 7b. Size-weighted diagram for 327 grains of sample B, > 10 - 6 - 4 - 2 - 0.

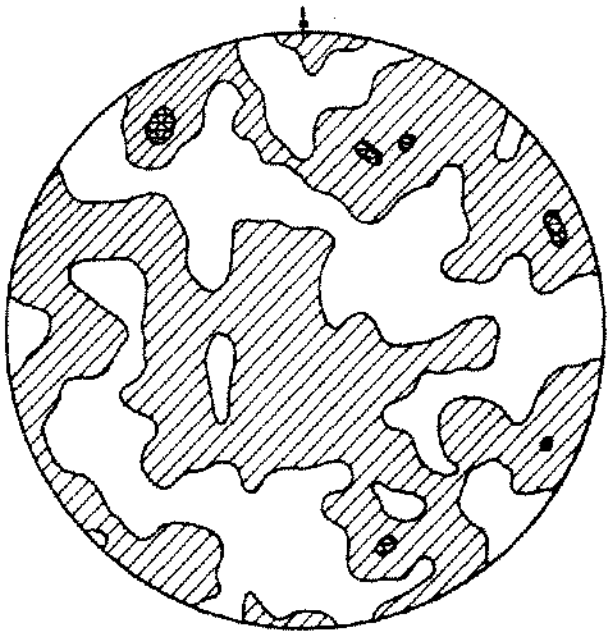

Figure 8a. Conventional diagram for 150 sylvite and 123 halite grains of sample C, > 2 - 1 - 0.

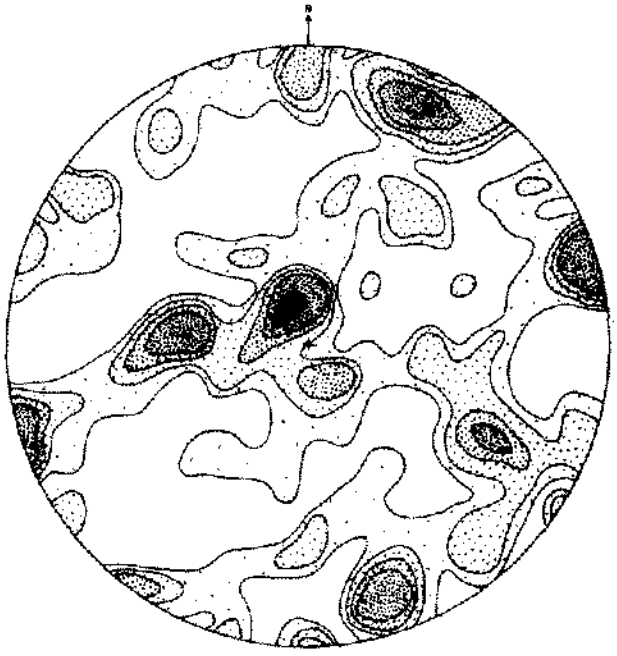

Figure 8b. Size-weighted diagram for 273 grains of sample C, > 20 - 10 - 6 - 4 - 2 - 0.

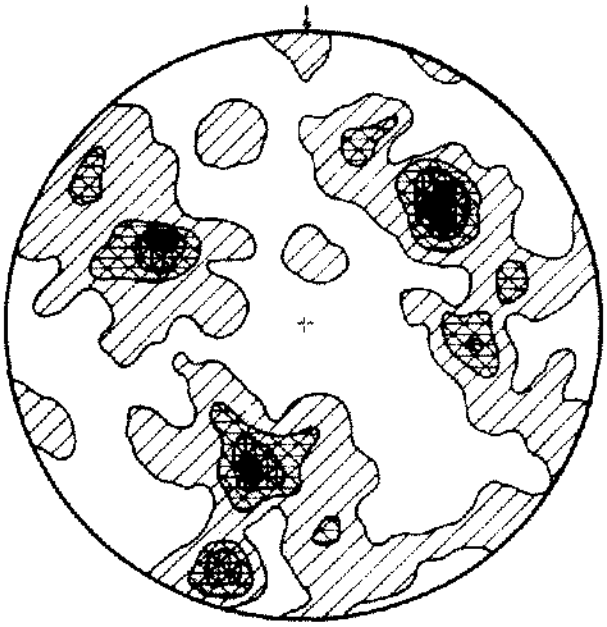

Figure 9a. Conventional diagram for 200 grains in the upper half of sample D, > 4 - 3 - 2 - 1 - 0.

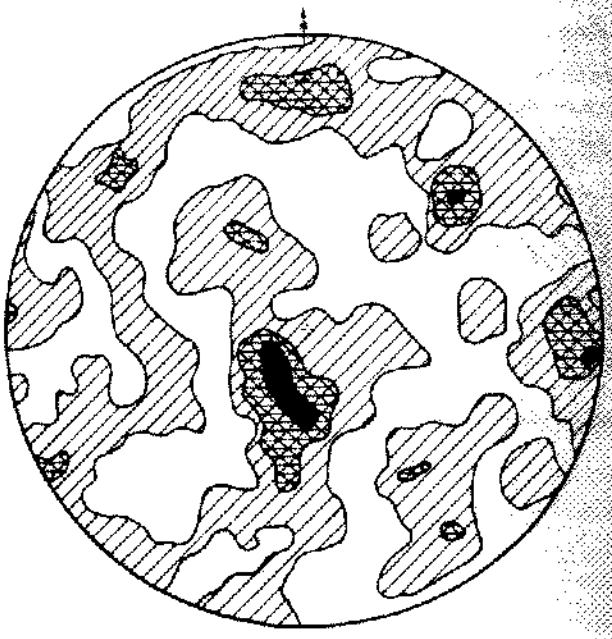

Figure 9b. Conventional diagram for 94 sylvite and 106 halite grains in the lower half of sample D, > 4 - 3 - 2 - 1 - 0.

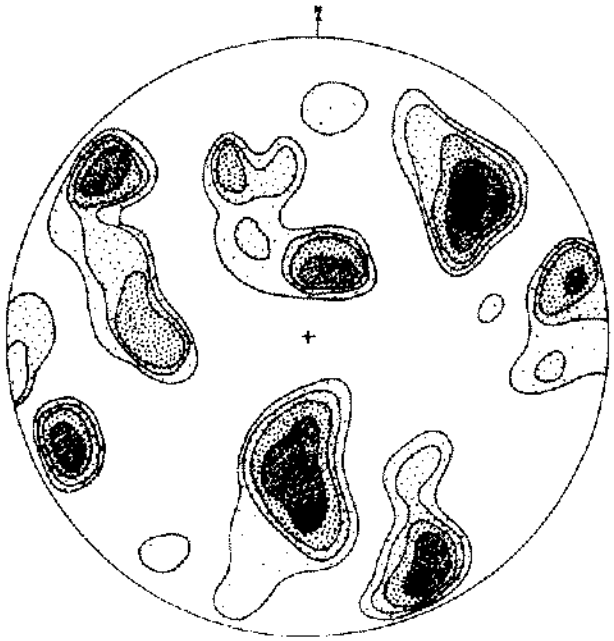

Figure 9c. Size-weighted diagram for the lower half of sample D (200 grains), > 15 - 10 - 6 - 4 - 2 - 0.

The crystallographic axes of sylvite and halite, in the actual fabrics, tend to be concentrated within three girdles along the principal stress planes. Maxima tend to form parallel, or subparallel, to the directions of principal stress.

So far, Kamb's theory has only been applied for crystal positions within the principal planes. Equations (1-3) and (4-6), for halite or sylvite, vary only with regard to the pressure difference. As the degree of preferred orientation within a girdle depends on the maximum potential differences, which are greatest in (2) and (5), the girdle normal to p_y will be the most imperfect. This effect gives rise to pronounced girdles normal to p_x and p_z, which are clearly developed in most of the petrofabric diagrams.

Figs. 2, 3, and 4 show that relatively few crystals occupy positions with [111] close to vertical. This can be explained on the basis of Kamb's theory if the chemical potentials $\mu_z^{[111]}$ and $\bar{\mu}^{[111]}$ are shown to be large. This can only be done by comparing $\mu_z^{[111]}$ and $\bar{\mu}^{[111]}$ with the minimum and maximum potentials in equations (1-6).

The minimal value of μ_z^{11} is confirmed if $\mu_z^{[111]} - \mu_z^{11}$ has a positive value (7a and 8a). For monomineralic fabrics $\bar{\mu}^{[111]} - \bar{\mu}^{11}$ should be positive (7b and 8b). Equations 7 determine the chemical potentials for [111] parallel to z, whereas (8a) and (8b) determine those for [111] parallel to x. The position of the three crystallographic axes for [111] parallel to z is shown in Fig. 14. The same figure can be used for [111] parallel to x, if x and z exchange their positions. Equations (7) and (8) were obtained from Kamb's (1959) equations (1, 9, 10, 11, 35).

$$\mu_z^{[111]} - \mu_z^{11} = V_o \left(-S_{11} + S_{12} + \frac{S_{44}}{2}\right)\left(\frac{1}{4}P_x^2 + \frac{1}{4}P_y^2 + \frac{1}{3}P_z^2 - \frac{1}{6}P_xP_y - \frac{1}{3}P_xP_z - \frac{1}{3}P_yP_z\right) \qquad (7a)$$

$$\bar{\mu}^{[111]} - \bar{\mu}^{11} = V_o \left(-S_{11} + S_{12} + \frac{S_{44}}{2}\right)\left(\frac{1}{4}P_x^2 + \frac{1}{4}P_y^2 + \frac{1}{3}P_z^2 - \frac{1}{6}P_xP_y - \frac{1}{3}P_xP_z - \frac{1}{3}P_yP_z\right) \qquad (7b)$$

$$\mu^{[111]} - \mu_x^{11} = V_o \left(-S_{11} + S_{12} + \frac{S_{44}}{2}\right)\left(\frac{1}{3}P_x^2 + \frac{1}{4}P_y^2 + \frac{1}{4}P_z^2 - \frac{1}{3}P_xP_y - \frac{1}{3}P_xP_z - \frac{1}{6}P_yP_z\right) \qquad (8a)$$

$$\bar{\mu}^{[111]} - \bar{\mu}^{11} = V_o \left(-S_{11} + S_{12} + \frac{S_{44}}{2}\right)\left(\frac{1}{3}P_x^2 + \frac{1}{4}P_y^2 + \frac{1}{4}P_z^2 - \frac{1}{3}P_xP_y - \frac{1}{3}P_xP_z - \frac{1}{6}P_yP_z\right) \qquad (8b)$$

In a general state of stress, the principal stresses can be split into a uniform stress (-p), equal in all directions, and a deviator with the principal stresses $\sigma_3 < \sigma_2 < \sigma_1$. As the principal pressures are the negatives of the principal stresses the following equations result:

$$\begin{aligned} p - \sigma_1 &= P_x \\ p - \sigma_2 &= P_y \\ p - \sigma_3 &= P_z \end{aligned} \qquad (9)$$

The principal stresses of any deviator can be expressed in terms of maximum shear stress τ and a quantity ν (Nadai, 1950, p. 106).

$$\begin{aligned} \sigma_1 &= \tau - \frac{\nu\tau}{3} \\ \sigma_2 &= \frac{2}{3}\nu\tau \\ \sigma_3 &= -\left(\tau + \frac{\nu\tau}{3}\right) \end{aligned} \qquad (10)$$

ν varies between:

$$-1 \le \nu \le 1 \qquad (11)$$

and is defined (Nadai, 1950, p. 106) as

$$\nu = \frac{2\sigma_2 - \sigma_1 - \sigma_3}{\sigma_1 - \sigma_3} \qquad (12)$$

By substituting the principal stresses in (9) with the expressions of (10), we obtain:

$$p_x = \rho - \tau + \frac{\nu\tau}{3}$$

$$p_y = \rho - \frac{2\nu\tau}{3} \qquad (13)$$

$$p_z = \rho + \tau + \frac{\nu\tau}{3}$$

Equations (7) and (9) can be expressed in terms of (13):

$$\mu_z^{[111]} - \mu_z^{111} = \left(-S_{11} + S_{12} + \frac{S_{44}}{2}\right)\tau^2\left(\frac{\nu^2}{4} + \frac{\nu}{6} + \frac{11}{12}\right)V_o \qquad (14a)$$

$$\bar{\mu}^{[111]} - \bar{\mu}^{111} = \left(-S_{11} + S_{12} + \frac{S_{44}}{2}\right)\tau^2\left(\frac{\nu^2}{4} + \frac{\nu}{6} + \frac{11}{12}\right)V_o \qquad (14b)$$

Similarly, (8a) and (8b) become:

$$\mu_z^{[111]} - \mu_z^{111} = \left(-S_{11} + S_{12} + \frac{S_{44}}{2}\right)\tau^2\left(\frac{\nu^2}{4} - \frac{\nu}{6} + \frac{11}{12}\right)V_o \qquad (15a)$$

$$\bar{\mu}^{[111]} - \bar{\mu}^{111} = \left(-S_{11} + S_{12} + \frac{S_{44}}{2}\right)\tau^2\left(\frac{\nu^2}{4} - \frac{\nu}{6} + \frac{11}{12}\right)V_o \qquad (15b)$$

As $(-s_{11} + s_{12} + \frac{s_{44}}{2})$ for halite and sylvite is positive, the potential differences in (14) and (15) are positive. Hence $\mu_z^{[111]}$ and $\bar{\mu}^{[111]}$ are greater than μ_z^{111} and $\bar{\mu}^{111}$.

In the case of pure shear, the principal pressures can be expressed in terms of the maximum shear stress τ, and a hydrostatic pressure p (Kamb, 1959, p. 167).

$$p_x = p - \tau$$
$$p_y = p \qquad (16)$$
$$p_z = p + \tau$$

Equations (14) and (15) can be written for pure shear ($\nu = 0$):

$$\mu_z^{[111]} - \mu_z^{111} = V_o\left(-S_{11} + S_{12} + \frac{S_{44}}{2}\right)\frac{11}{12}\tau^2 \qquad (17)$$

$$\bar{\mu}^{[111]} - \bar{\mu}^{111} = V_o\left(-S_{11} + S_{12} + \frac{S_{44}}{2}\right)\frac{11}{12}\tau^2 \qquad (18)$$

It is of interest to determine whether $\mu_z^{[111]}$ and $\bar{\mu}^{[111]}$ are high chemical potentials in comparison with the maximum potentials in (1-6). If this should be the case, the petrofabric diagrams (Fig. 3) could be explained on the basis of Kamb's theory. The maximum potential differences derived from equations (1-6) are those for $\alpha = \frac{\pi}{4}$. V_o and $(-S_{11} + S_{12} + \frac{S_{44}}{2})$ in equations (1-6) are equal for a given mineral. Hence equations (2) and (5), containing the maximum difference of the principal pressures, express the greatest potential difference, while equations (3) and (6) express the potential difference in the best-developed girdle.

If the fabric diagrams are to explained fully on the basis of Kamb's theory, the maximum potential within the best-developed girdle must be smaller than $\mu_z^{[111]}$ and $\bar{\mu}^{[111]}$. Equations (2, 3,

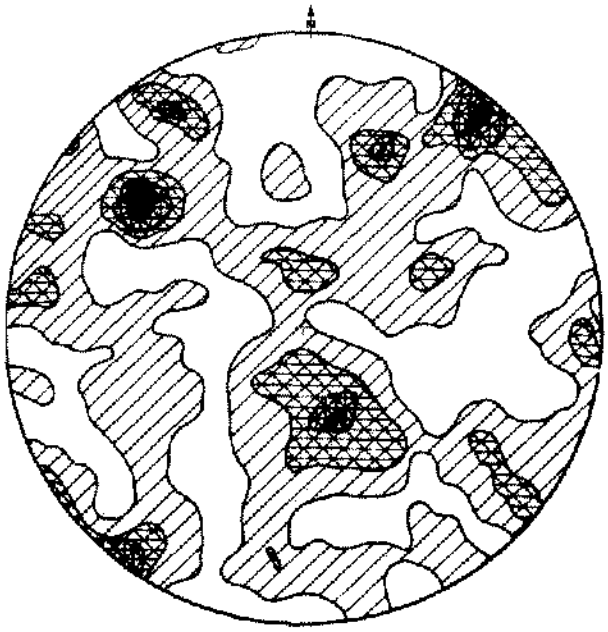

Figure 10a. Conventional diagram for 66 sylvite and 44 halite grains (> 0.75 inches across) in sample E, > 4 - 3 - 2 - 1 - 0.

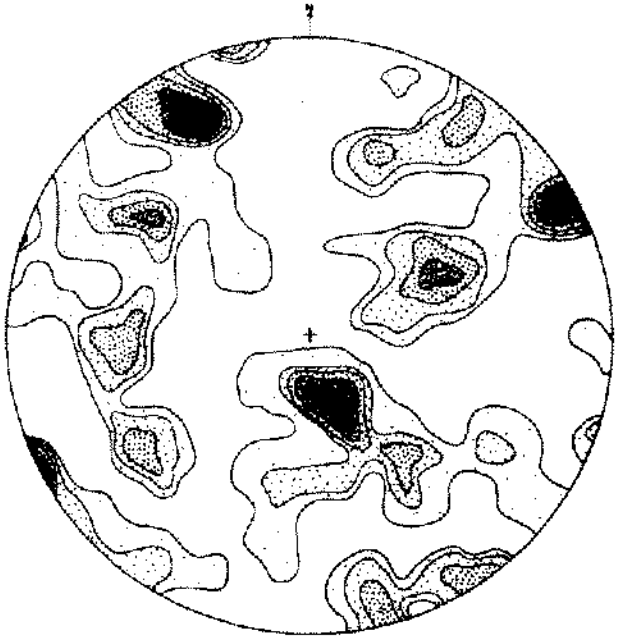

Figure 10b. Size-weighted diagram for the 110 large grains of sample E, > 30 - 10 - 6 - 4 - 2 - 0.

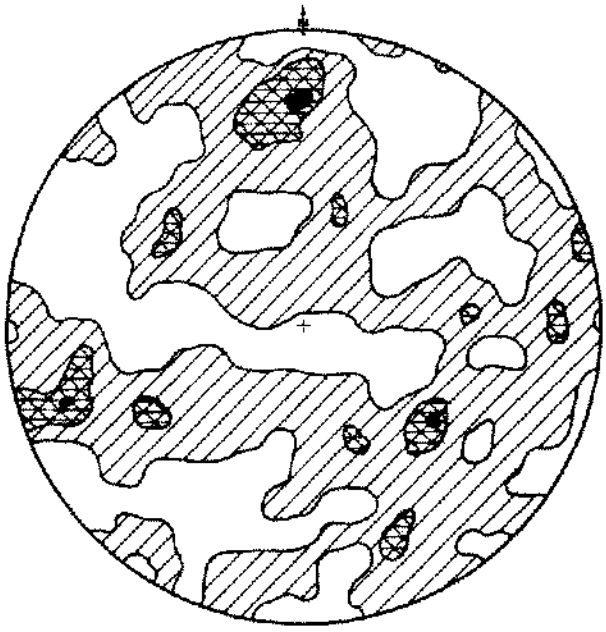

Figure 11a. Conventional diagram for 31 sylvite and 172 halite grains of sample F, > 3 - 2 - 1 - 0.

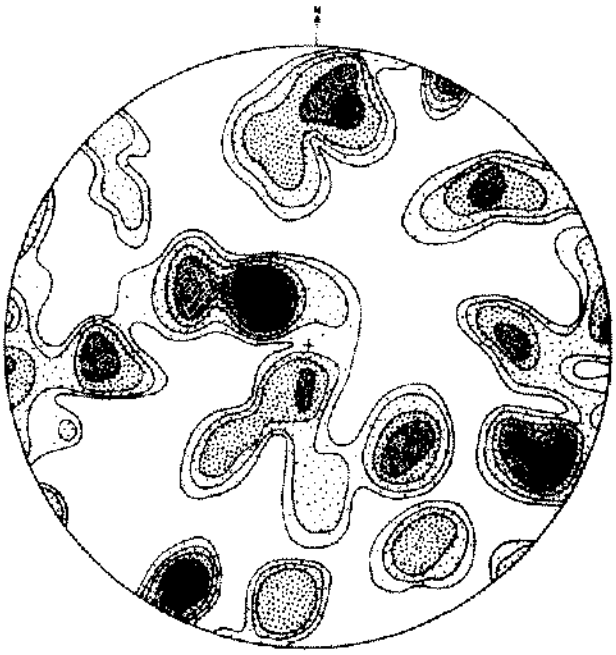

Figure 11b. Size-weighted diagram for 203 grains of sample F, > 15 - 10 - 6 - 4 - 2 - 0.

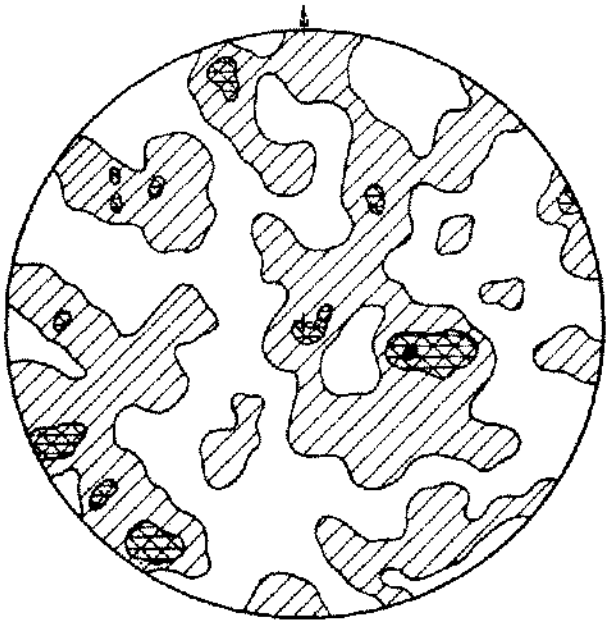

Figure 12a. Conventional diagram for 177 halite and 48 sylvite grains of sample G, > 3 - 2 - 1 - 0.

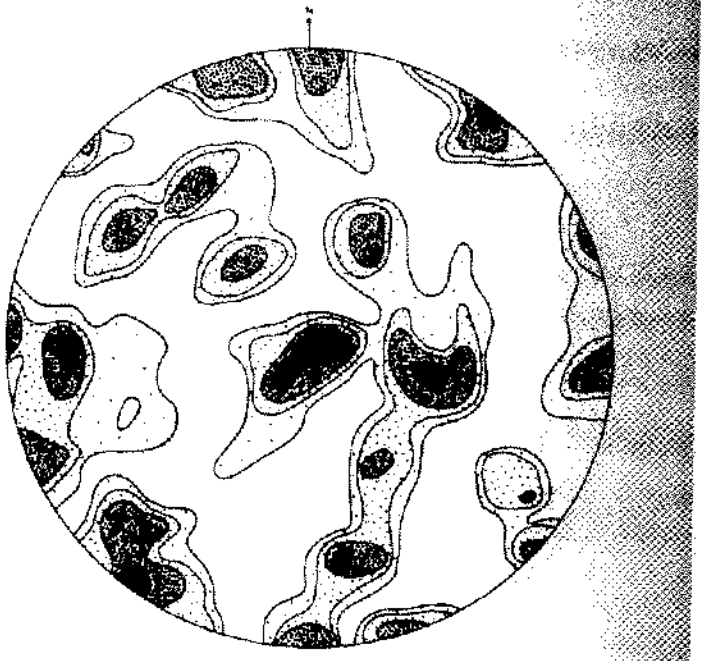

Figure 12b. Size-weighted diagram for 225 grains of sample G, > 10 - 6 - 4 - 2 - 0.

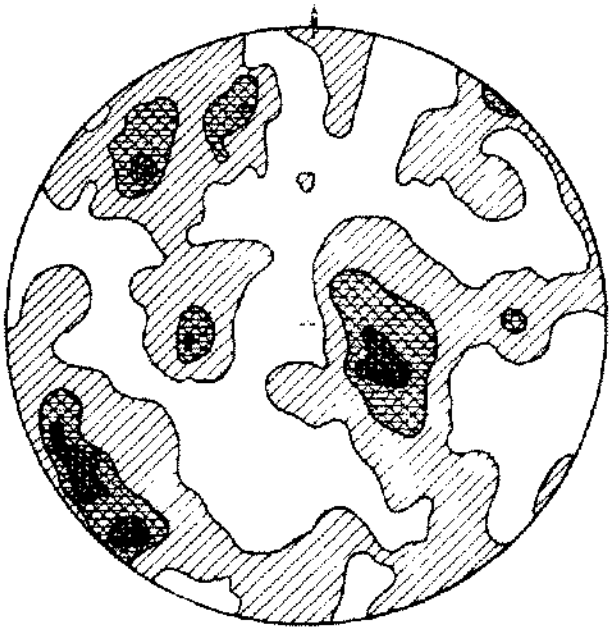

Figure 13a. Conventional diagram for 120 halite grains in the lower half of sample H, > 4 - 3 - 2 - 1 - 0.

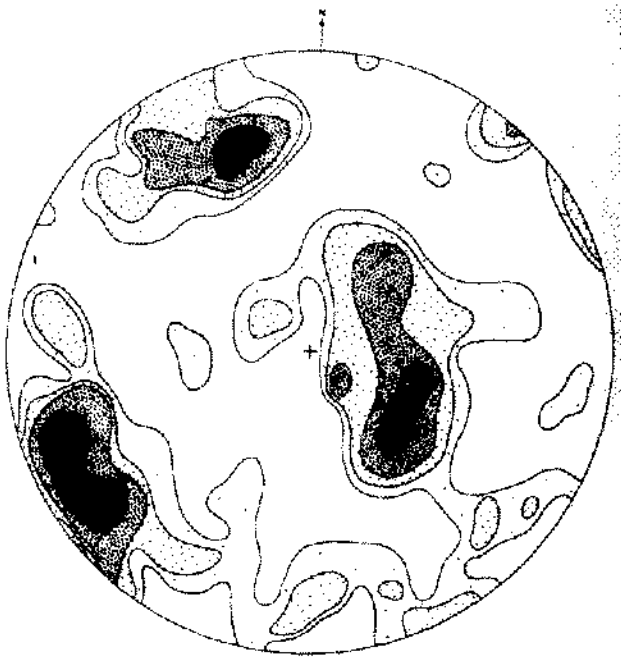

Figure 13b. Size-weighted diagram for 120 halite grains in lower half of sample H, > 10 - 6 - 4 - 2 - 0.

, 6, 14, 15, 17, 18) can be used to determine the relative values of $\mu_z^{[111]}$ and $\mu_z^{[11]}$. When substituting for $(p_x - p_y)$ and $(p_x - p_z)$ in (2) and (3), by means of (13) and (16), we first obtain for a eneral state of stress:

$$\sin^2\frac{\pi}{4}\cos^2\frac{\pi}{4}\left(p_x - p_y\right)^2 = \tau^2\left(\frac{\nu}{2} - \frac{1}{2}\right)^2 \tag{19}$$

for best-developed girdle)

$$\sin^2\frac{\pi}{4}\cos^2\frac{\pi}{4}\left(p_x - p_z\right)^2 = \tau^2 \tag{20}$$

for least-developed girdle)

$\tau^2\left(\frac{\nu}{2} - \frac{1}{2}\right)^2$ and τ^2 are to be compared with the quantities $\tau^2\left(\frac{\nu^2}{4} + \frac{\nu}{6} + \frac{11}{12}\right)$ and $\tau^2\left(\frac{\nu^2}{4} - \frac{\nu}{6} + \frac{11}{12}\right)$ 'rom equations (14) and (15). ν is determined by (11) and (12) in a general state of stress.

For $\nu = -1$:

$$\tau^2\left(\frac{\nu}{2} - \frac{1}{2}\right)^2 = \tau^2\left(\frac{\nu^2}{4} + \frac{\nu}{6} + \frac{11}{12}\right) < \tau^2\left(\frac{\nu^2}{4} - \frac{\nu}{6} + \frac{11}{12}\right)$$

and for $\nu > -1$

$$\tau^2\left(\frac{\nu^2}{4} - \frac{\nu}{6} + \frac{11}{12}\right) > \tau^2\left(\frac{\nu}{2} - \frac{1}{2}\right)^2 < \tau^2\left(\frac{\nu^2}{2} + \frac{\nu}{6} + \frac{11}{12}\right) \tag{21}$$

It follows that $\mu_z^{[111]}$ and $\mu^{[111]}$, in all triaxial states of stress, are greater than the maximum potential along the best-developed girdle (Fig. 3). For $\nu = -1$, $\sigma_2 = \sigma_3$ (Nadai, 1950, p. 107), which implies a uniaxial state of stress. A similar procedure for the least-developed girdle yields:

for $-1 \le \nu < -\frac{1}{3}$ $\qquad 1 < \frac{\nu^2}{4} - \frac{\nu}{6} + \frac{11}{12}$ (22a)

and for $-\frac{1}{3} < \nu < 1$ $\qquad 1 > \frac{\nu^2}{4} - \frac{\nu}{6} + \frac{11}{12}$ (22b)

and for $\frac{1}{3} < \nu \le 1$ $\qquad 1 < \frac{\nu^2}{4} + \frac{\nu}{6} + \frac{11}{12}$ (23)

and for $-1 \le \nu < \frac{1}{3}$ $\qquad 1 > \frac{\nu^2}{4} + \frac{\nu}{6} + \frac{11}{12}$ (24)

In the case of pure shear, we have:

$$\tau^2 > \frac{11}{12}\tau^2 \tag{25}$$

It follows that the relative values of $\mu_z^{[111]}$ and $\bar{\mu}^{[111]}$ depend on the principal stresses, which are unknown. However, the maximum potential along the best-developed girdle is smaller than $\mu_z^{[111]}$ and $\bar{\mu}^{[111]}$ in all states of triaxial stress. All values for $\mu_z^{[111]}$ and $\bar{\mu}^{[111]}$ are relatively close to the maximum potential along the least-developed girdle. In many states of triaxial stress $\mu_z^{[111]}$ and $\bar{\mu}^{[111]}$ appear to be absolute maxima.

Kamb (1959, p. 166) has pointed out that definite crystal shapes develop during competitive growth in each of the two fabric environments distinguished above. The first type of crystal

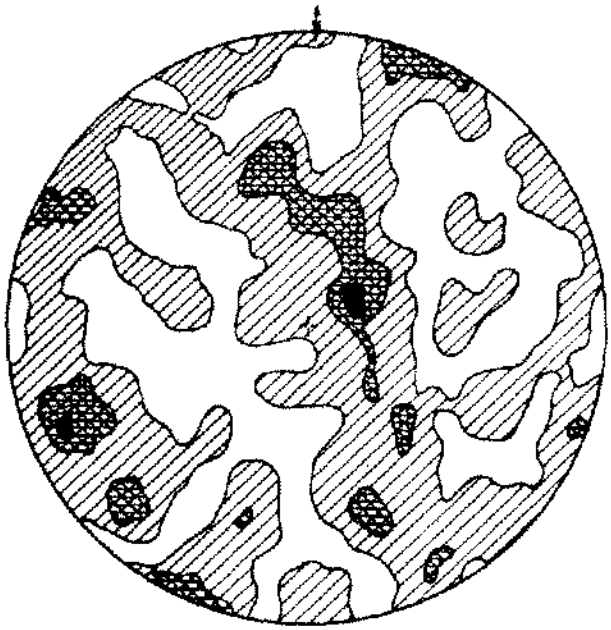

Figure 13c. Conventional diagram for 127 halite grains in the upper half of sample H. > 3 - 2 - 1 - 0.

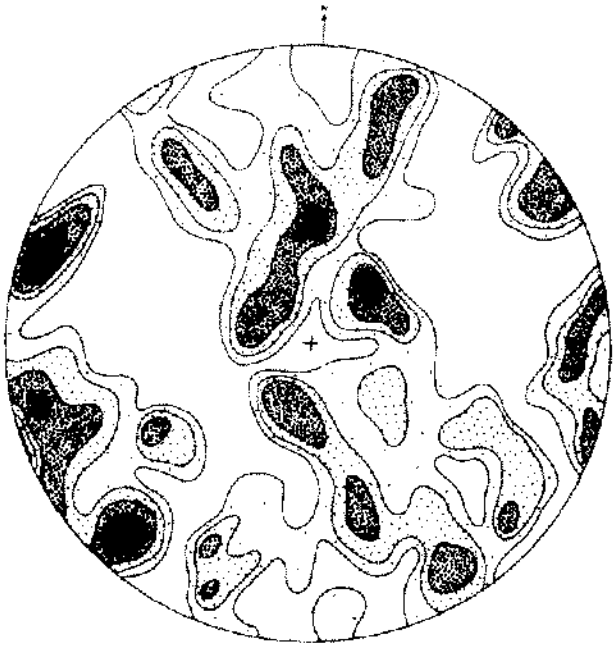

Figure 13d. Size-weighted diagram for 127 halite grains in the upper half of sample H. > 10 - 6 - 4 - 2 - 0.

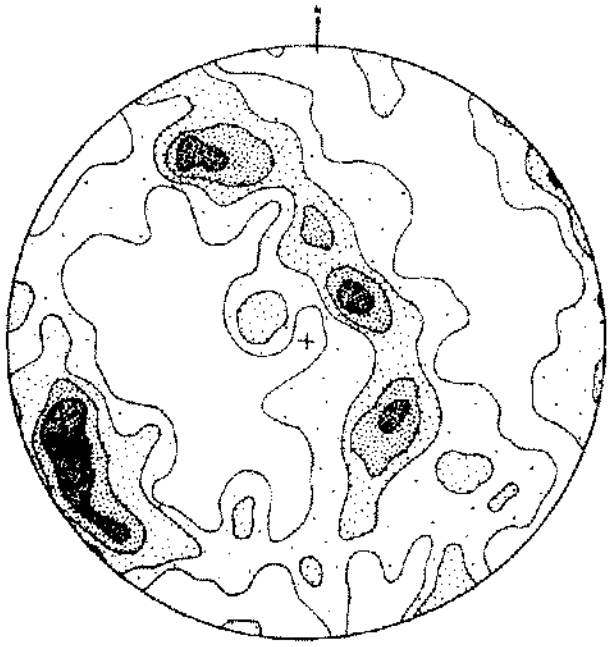

Figure 13e. Conventional diagram for 70 large halite grains (> 0.75 inches across) in the total sample H. > 5 - 4 - 3 - 2 - 1 - 0.

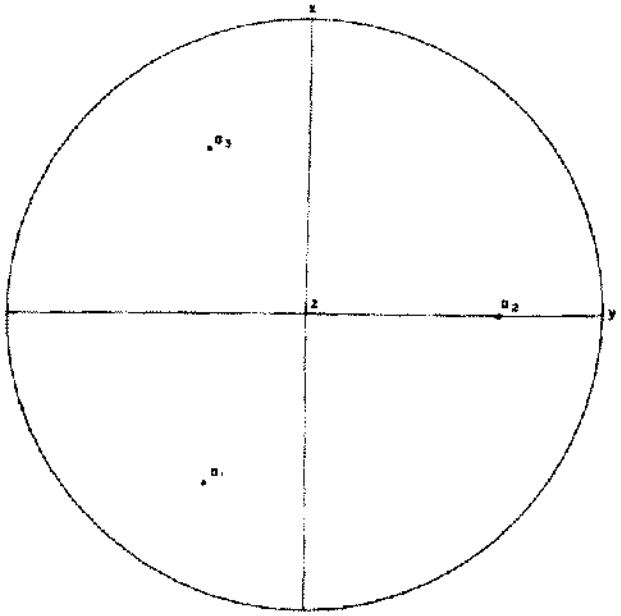

Figure 14. Arbitrarily chosen position of the crystallographic axes for [111] parallel to z.

growth proceeds in a monomineralic fabric with intercrystalline fluid, or in a polycrystalline fabric with, or without, intercrystalline fluids. The second type of competitive crystal growth takes place in monomineralic fabrics without intercrystalline fluids (Kamb, 1959, section VI).

Crystal growth of the first type tends to produce crystals which are flattened normal to the greatest pressure. Growth of the second type leads to grain shapes which depend on the shape and fabric of the initial grains, as well as on the state of stress.

For initially equant grains in a monomineralic rock, Kamb (1959, p. 164) predicted the average shape for grains which have grown in preferred directions. Suppose the chemical potential across an interface is $\mu\ (\omega,\ \eta)$ where η is the vector normal to the interface, and ω indicates collectively the various orientation parameters of the crystal. Across this interface the first crystal sees, on the average, a second crystal that requires a chemical potential $\bar{\mu}\ (\eta)$, which is $\mu\ (\omega,\ \eta)$ averaged with proper weighting over all orientations ω in the original fabric. If $\mu\ (\omega,\ \eta) < \bar{\mu}\ (\eta)$ the first grain, of orientation ω, will tend to grow, on the average, at the expense of the second grain, across the common interface η.

To a first approximation, the rate of growth, $\frac{\alpha r\ (\omega,\ \eta)}{\alpha t}$, may be considered as proportional to the chemical potential difference (Kamb, 1959, equ. 29):

$$\frac{\alpha r\ (\omega,\ \eta)}{\alpha t} = -\,C\left[\mu\ (\omega,\ \eta) - \bar{\mu}\ (\eta)\right] \tag{26}$$

To apply (26) to the preferred orientation of halite and sylvite ([[100]] parallel to the principal stresses), let us assume that the original fabric consisted of equant grains with uniformly scattered orientations. We then obtain:

$$\begin{aligned}
\bar{\mu}_z &= \frac{\mu_z\ (\max) + \mu_z\ (\min)}{2} \\
\bar{\mu}_y &= \frac{\mu_y\ (\max) + \mu_y\ (\min)}{2} \\
\bar{\mu}_x &= \frac{\mu_x\ (\max) + \mu_x\ (\min)}{2}
\end{aligned} \tag{27}$$

For most triaxial states of stress $\mu_z\left(\frac{\pi}{4}\right)$, $\mu_y\left(\frac{\pi}{4}\right)$ and $\mu_x\left(\frac{\pi}{4}\right)$, in the principal plane (xz) perpendicular to p_y, are maximum potentials, while μ_z^{μ}, μ_y^{μ} and μ_x^{μ} are always minima. From equations (26) and (27) we obtain:

$$\begin{aligned}
\frac{\alpha r\ (100_{\perp}z)}{\alpha t} &= -\,C\left[\mu_z^{\mu} - \frac{\mu_z\left(\frac{\pi}{4}\right) + \mu_z^{\mu}}{2}\right] = -\,C\left[\frac{\mu_z^{\mu} - \mu_z\left(\frac{\pi}{4}\right)}{2}\right] \\
\frac{\alpha r\ (100_{\perp}y)}{\alpha t} &= -\,C\left[\mu_y^{\mu} - \frac{\mu_y\left(\frac{\pi}{4}\right) + \mu_y^{\mu}}{2}\right] = -\,C\left[\frac{\mu_y^{\mu} - \mu_y\left(\frac{\pi}{4}\right)}{2}\right] \\
\frac{\alpha r\ (100_{\perp}x)}{\alpha t} &= -\,C\left[\mu_x^{\mu} - \frac{\mu_x\left(\frac{\pi}{4}\right) + \mu_x^{\mu}}{2}\right] = -\,C\left[\frac{\mu_x^{\mu} - \mu_x\left(\frac{\pi}{4}\right)}{2}\right]
\end{aligned} \tag{28}$$

$$\left[\mu_z^{\mu} - \mu_z\left(\frac{\pi}{4}\right)\right] = \left[\mu_y^{\mu} - \mu_y\left(\frac{\pi}{4}\right)\right] = \left[\mu_x - \mu_x\left(\frac{\pi}{4}\right)\right] \tag{29}$$

Hence, halite grains, as well as sylvite grains, tend to grow at equal rates into the three principal directions, and equant grains result.

Wardlaw (1964) has presented evidence that primary halite in salt rocks developed a preferred orientation with [111] normal to bedding. If all grains had achieved this position:

$$\bar{\mu}_z = \mu_z^{[111]} \qquad \bar{\mu}_y = \mu_y^{[111]} \qquad \bar{\mu}_x = \mu_x^{[111]} \tag{30}$$

As, $\mu_z^{\mu} - \mu_z^{[111]} = \mu_y^{\mu} - \mu_y^{[111]} = \mu_x^{\mu} - \mu_x^{[111]}$. (31)

the halite grains in pure salt rocks, which recrystallized according to Kamb's theory, would be equant.

In the sylvinites of Esterhazy, the halite grains commonly occur in clusters surrounded by sylvite. This suggests that there was no uniform distribution of halite and sylvite prior to deformation and that neither of the two principal types of growth took place alone, but rather a combination of both.

The sylvite and halite grains in all samples are approximately equant, as predicted by Kamb's theory. The sylvite grains, which form a better defined pattern than halite in the composite diagrams, are generally larger than the halite grains. Both the better defined fabric, and the larger grain size of sylvite, can be explained by the higher value of $(-s_{11} + s_{12} + \frac{s_{44}}{2})$ for sylvite in equations (1-8) and (28).

CONCLUSIONS

The halite and sylvite grains, in all the samples analyzed, have a preferred orientation which is most pronounced in the weighted diagrams. All fabric diagrams exhibit a pseudo-orthorhombic symmetry. The crystallographic axes of halite and sylvite tend to align with the axes of gentle large-scale folds, and there is commonly a pronounced girdle parallel to the axial planes.

It is concluded that the observed fabrics are a result of syntectonic crystallization in the quasi-horizontal sylvinite rocks. The patterns of preferred orientation, and the observed grain shapes, can be fully explained on the basis of Kamb's theory which predicts a schematic fabric pattern as in Fig. 2. Kamb's thermodynamic theory predicts:

1. three major maxima parallel to the principal stress axes;
2. the major minima in Fig. 2 or Fig. 3;
3. two rather complete girdles parallel to (xy) and (yz);
4. one incomplete girdle parallel to (xz);
5. the minimum density in each girdle at 45 degrees to the principal axes;
6. identical fabric patterns for sylvite and halite as well as a higher degree of preferred orientation for sylvite;
7. rather equant grains of both halite and sylvite, the latter being larger on the average.

The maximum at 50 degrees in the (xz) girdle of Fig. 4 does not conform completely with the predictions listed above. However, the girdle narrows considerably at roughly 45 degrees, which suggests that the maximum under consideration may be due to inhomogeneities in the fabric.

REFERENCES

Barrett, C. S., 1952, The structure of metals: McGraw-Hill Book Co., New York.

Carey, S. W., 1953, The rheid concept in geotectonics: Geol. Soc. Australia Jour., vol. 1, pp. 67-116.

_____, 1962, Folding: Alberta Soc. Petroleum Geologists Jour., vol. 10, p. 98.

Chayes, F., 1949, in Fairbairn, H. W., Structural petrology of deformed rocks: Addison Wesley Press, Inc., Cambridge, Mass.

Clabaugh, P. S., 1962, Petrofabric study of deformed salt: Science, vol. 136, no. 3514, pp. 389-391.

Engels, B., 1959, Die kleintektonische Arbeitsweise unter besonderer Beruecksichtigung ihrer Anwendung im deutschen Palaeozoikum: Geotektonische Forschungen, Heft 13, pp. 43-45, Schweizerbartsche Verlagsbuchhandlung, Stuttgart.

Flinn, D., 1958, On tests of significance of preferred orientation in three-dimensional fabric diagrams: Jour. Geology, vol. 66, pp. 526-539.

Haff, J.C., 1938, Preparation of petrofabric diagrams: Am. Mineralogist, vol. 23, pp. 543-574.

Ingerson, E., 1940, Fabric criteria for distinguishing pseudo ripple marks from ripple marks: Geol. Soc. America Bull., vol. 51, pp. 557-570.

Kamb, W.B., 1959, Theory of preferred crystal orientation developed by crystallization under stress: Jour. Geology, vol. 67, pp. 153-170.

_____, 1961, The thermodynamic theory of non-hydrostatically stressed solids: Jour. Geophys. Research, vol. 66, pp. 259-271.

Mellis, O., 1942, Gefuegediagramme in stereographischer Projektion: Min. Pet. Mitt., vol. 53, pp. 331-353.

Nadai, A., 1950, Theory of flow and fracture of solids: McGraw-Hill Book Co., New York.

Nye, J.F., 1960, Physical properties of crystals: At the Clarendon Press, Oxford, p. 160, table 9.

Odé, H., 1962, International Conference on Saline Deposits, Houston, Texas, Work Sessions.

Plank, A. van der, 1962, Petrology and geochemistry of some diamond drill cores from the Saskatchewan potash deposits: Unpublished M. Sc. thesis, University of Wisconsin.

Sander, B., 1948, Einfuehrung in die Gefuegekunde der geologischen Koerper, I. Teil: Springer Verlag, Vienna.

Schwerdtner, W.M., 1964, Genesis of potash rocks in Middle Devonian Prairie Evaporite Formation of Saskatchewan: Am. Assoc. Petroleum Geologists Bull., vol. 48, pp. 1108-1115.

Serata, S., and Gloyna, E.F., 1960, Principles of structural stability of underground salt cavities: Jour. Geophys. Research, vol. 65, pp. 2979-2887.

Turner, F.J., and Weiss, L.E., 1963, Structural analysis of metamorphic tectonites: McGraw-Hill Book Co., New York.

Wardlaw, N.C., 1964, Bromide in some Middle Devonian salt rocks of Alberta and Saskatchewan: 3rd Internat. Williston Basin Symposium Proceedings, Billings Geol. Soc., Montana, pp. 270-273.